Organic ligands and CeO_2-Induced Generic Valence Modulation Strategy to Design Fe Active Sites for Promoted Oxygen Involved Reaction in Rechargeable Zinc-Air Batteries

Jiao Peng[a,1], Zining Wang[b,1], Jianwei Ren[c]*, Yudong He[a], Jiahao Li[a], Shichang Xin[a], Xuyun Wang[a], Hui Wang[a]*and Rongfang Wang[a]*

[a] State Key Laboratory Base for Eco-Chemical Engineering, College of Chemical Engineering, Qingdao University of Science and Technology, Qingdao, 266042, China.

[b] School of Chemical Science and Engineer, Tongji University, 1239 Siping Road, Shanghai 200092, China.

[c] Department of Chemical Engineering, University of Pretoria, cnr Lynnwood Road and Roper Street, Hatfield 0028, South Africa.

[1] Contribute equally.
* Corresponding author.
E-mail addresses: jianwei.ren@up.ac.za (J. Ren), wangh@qust.edu.cn (H. Wang), rfwang@qust.edu.cn (R. Wang).

Materials

Ferrous chloride tetrahydrate ($FeCl_2·4H_2O$, ≥99%), peptone (total nitrogen ≥14.5%, amino nitrogen ≥2.5%), calcium chloride ($CaCl_2$, ≥99%), anhydrous phenanthroline ($C_{12}H_8N_2·H_2O$), cerium ammonium nitrate ($Ce(NH_4)_2(NO_3)_6$), and hydrochloric acid (HCl) were obtained from Sinopharm Chemical Reagent Co., Ltd. All reagents used were of analytical grade and were employed directly without further purification. Nitrogen (N_2, 99.999%) and oxygen (O_2, 99.999%) were sourced from Qingdao Ludong Gas Co., Ltd.

Physical Characteristics

X-ray diffraction (XRD) patterns were obtained using a Shimadzu XD-3A instrument, utilizing filtered Cu-Kα radiation (λ = 0.15418 nm) at 40 kV and 30 mA. Scanning was performed at a rate of 5° min^{-1} over a 2θ range of 10° to 90°. The surface morphology of the samples was analyzed with a Carl Zeiss Ultra Plus system scanning electron microscope (SEM). Transmission electron microscopy (TEM), high-resolution TEM (HRTEM), and selected area

electron diffraction (SAED) were carried out using a 300 kV FEI Tecnai G2 F30 field-emission transmission electron microscope, with microstructural characterization performed through an EDAX Genesis energy dispersive X-ray spectroscopy (EDX) system. X-ray photoelectron spectroscopy (XPS) was conducted on a VG ESCALAB 210 spectrometer, equipped with an MG 300 W X-ray source. Raman spectroscopy was recorded using a Bruker RFS 100 Raman spectrometer, with a 532 nm excitation laser. In situ Raman spectra under electrochemical ORR testing conditions were collected using a Horiba LabRam Aramis HR Evolution confocal Raman spectrometer, employing a 633 nm laser, with potential values converted to the reversible hydrogen electrode (RHE) scale. Ultraviolet photoelectron spectroscopy (UPS) was performed on a Thermo Scientific Nexsa G2 system, utilizing a He I excitation source. The specific surface area of the samples was measured using Brunauer-Emmett-Teller (BET) analysis, and pore size distribution was derived from density functional theory (DFT).

Electrochemical Evaluation

Electrochemical measurements were carried out using a CHI760D electrochemical analyzer (CH Instruments) with a three-electrode system. The counter electrode was a carbon rod, the reference electrode was Hg/HgO, and the working electrode consisted of a catalyst deposited onto nickel foam. The preparation of the working electrode involved dispersing 3 mg of the catalyst into 600 μL of a Nafion ethanol solution (0.25 wt.%) and sonicating for 30 min to form a homogeneous slurry. This slurry was then drop-cast onto a 1 cm × 1 cm piece of nickel foam. A 1.0 M KOH aqueous solution served as the electrolyte for the oxygen evolution reaction (OER) electrochemical testing. Potentials were converted to the reversible hydrogen electrode (RHE) scale using the equation:

$$E_{RHE} = E_{Hg/HgO} + 0.059\ pH + 0.098V \quad (1)$$

For further testing, a glassy carbon electrode (diameter 5.5 mm) was coated with the catalyst and used as the working electrode, with an Ag/AgCl electrode as the reference and a Pt wire as the counter electrode. The working electrode preparation involved dispersing 2 mg of the catalyst in 0.4 mL of Nafion ethanol solution (0.25 wt.%) and sonicating for 30 min to form a homogeneous slurry. Then, 8 mL of ink containing 40 mg of the catalyst was drop-cast onto the polished surface of a glassy carbon rotating disk electrode (catalyst loading: 0.196 mg

cm^{-2}) and air-dried. Prior to electrochemical measurements, the 0.1 M KOH electrolyte was purged with N_2 or O_2 for 30 min to achieve saturation for the oxygen reduction reaction (ORR) testing. The recorded potential values were converted to the RHE scale using the equation:

$$E_{RHE} = E_{Ag/AgCl} + 0.059\,pH + 0.197\,V \quad (2)$$

The accelerated durability test (ADT) for ORR was conducted within the voltage range of -0.36 to 0.13 V, using a scan rate of 50 mV s^{-1} and a rotation speed of 1600 rpm. The ORR stability was evaluated by comparing the linear sweep voltammetry (LSV) curves before and after 5500 cycles of cyclic voltammetry (CV) testing. For the OER process, the ADT test was performed within the voltage range of 1.02 to 1.12 V, using 5500 CV cycles with a scan rate of 50 mV s^{-1}.

The electron transfer number and H_2O_2 yield for ORR were determined using a rotating ring-disk electrode (RRDE), with calculations based on the following equations:

$$n = 4I_d/(I_d + I_r/N) \quad (3)$$

$$H_2O_2\% = 200I_r/(I_dN + I_r) \quad (4)$$

In these equations, I_d and I_r correspond to the disk current and ring current, respectively. The actual collection efficiency of the Pt ring (N) was determined to be 0.37 in the tests.

Zinc-Air Battery Testing

The zinc-air battery (ZAB) was assembled using a catalyst-coated nickel foam as the air cathode. The preparation procedure was as follows: 4 mg of the catalyst, 3 μL of polymer binder PTFE, 2 mg of conductive carbon black, and 2 mg of carbon powder were dispersed in 300 μL of isopropanol to form a uniform slurry. This slurry was then pressed onto the nickel foam under 20 MPa of pressure and dried in an oven at 60 °C to produce the electrode. A 1 mm thick, 1 cm wide 99.99% zinc foil was used as the anode, with a 0.2 M $Zn(OAc)_2$ and 6 M KOH solution serving as the electrolyte. For comparison purposes, a Pt/C + RuO_2 air cathode catalyst was prepared by combining 2 mg of commercial Pt/C (40 wt.%, Johnson Matthey) with 2 mg of commercial RuO_2. ZAB tests were performed using a Blue Electric Battery Tester.

Constant current discharge curves were recorded at a current density of 10 mA cm^{-2}, with the zinc foil being replaced regularly.

Table S1. The molar content ratio of Fe and Ce metals in the samples

Samples	n(mmol) of Fe	n(mmol) of Ce	n(Fe): n(Ce)
CeO_2-Fe_xO/NC-1	0.02	0.001	20:1
CeO_2-Fe_xO/NC-2	0.02	0.002	10:1
CeO_2-Fe_xO/NC-3	0.02	0.005	4:1
CeO_2-Fe_xO/NC-4	0.02	0.01	2:1

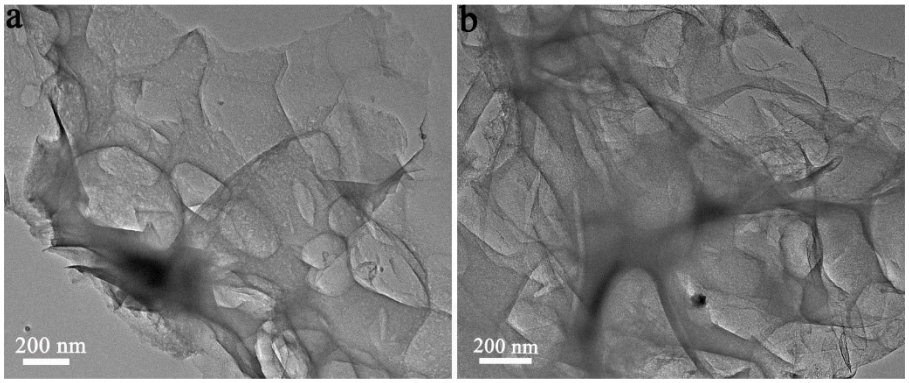

Fig. S1. TEM images of Ce-Fe_xO/NC sample.

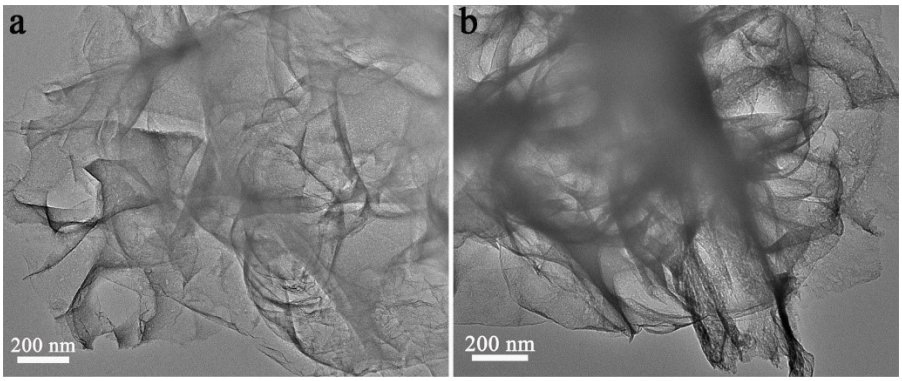

Fig. S2. TEM images of NC sample.

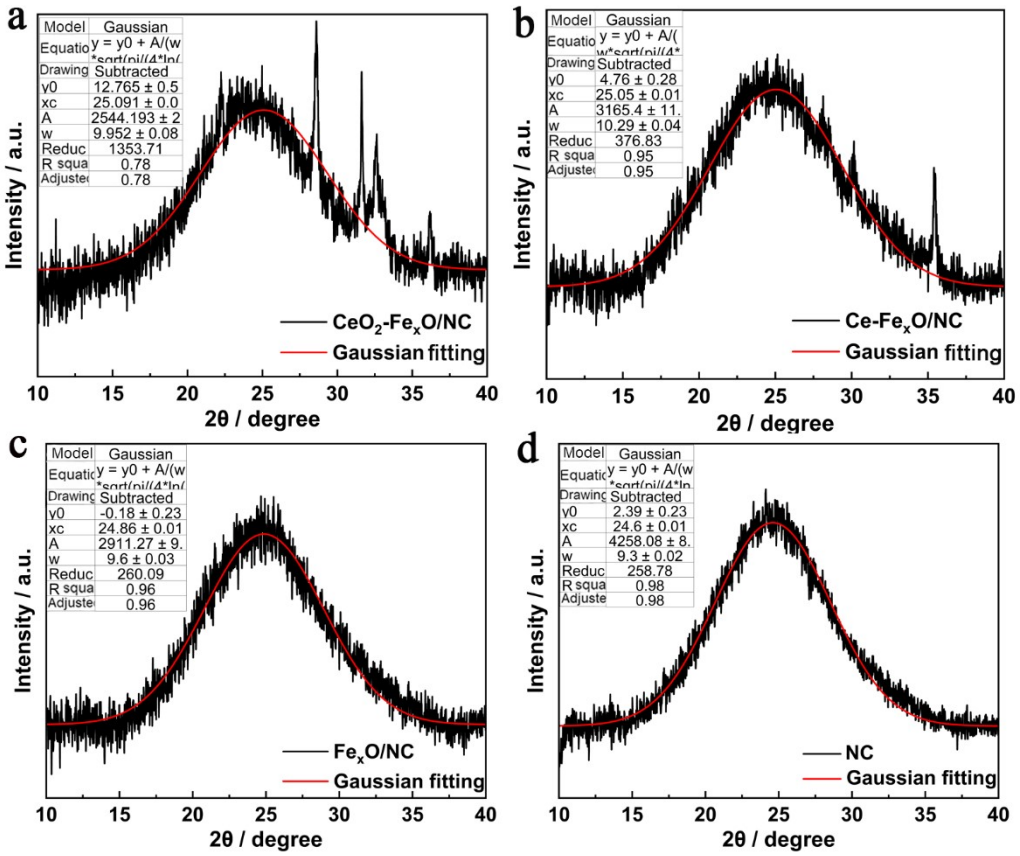

Fig. S3. The fitting plots obtained from Gaussian calculations in Origin Software for the (a) CeO_2-Fe_xO/NC, (b), Ce-Fe_xO/NC, (c) Fe_xO/NC, and (d) NC samples.

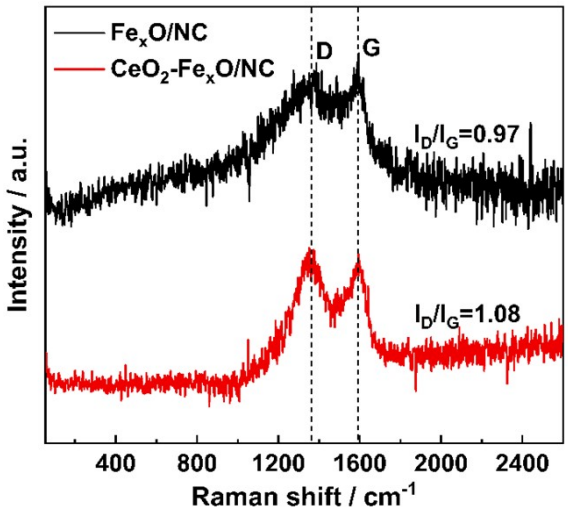

Fig. S4. Raman spectra of Fe_xO/NC and CeO_2-Fe_xO/NC samples.

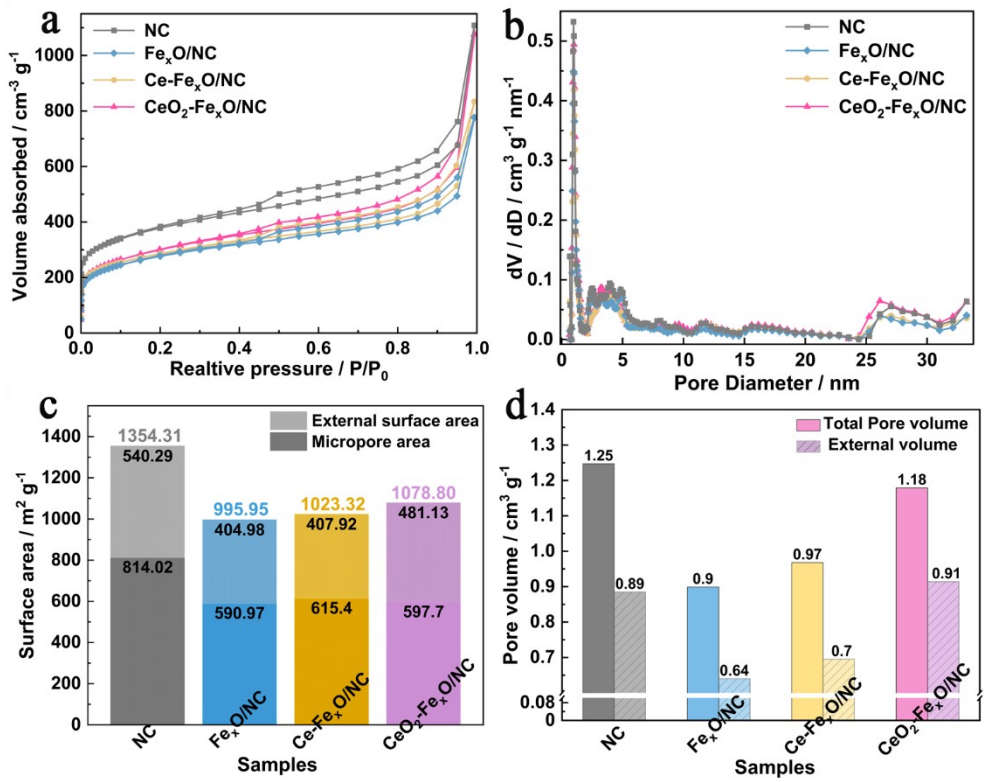

Fig. S5. (a) N_2 adsorption-desorption isotherm, (b) pore size distribution, (c) specific surface area distribution, and (d) pore volume distribution.

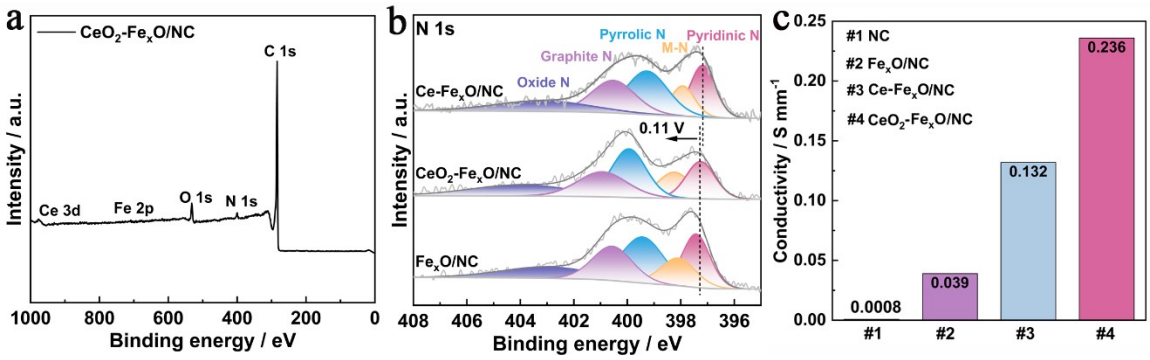

Fig. S6. (a) XPS full spectrum, (b) N 1s spectrum, and (c) Conductivities of the prepared samples.

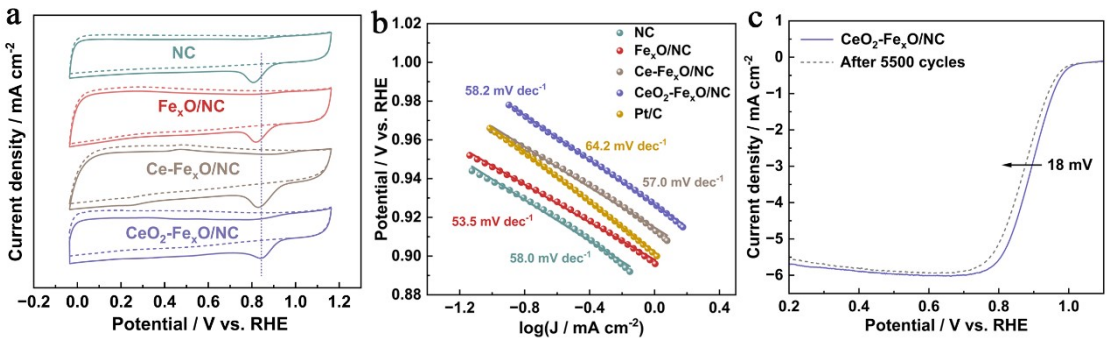

Fig. S7. ORR performance: (a) Cyclic voltammogram (CV), (b) Tafel fitting plot, and (c) Polarization curves of CeO_2-Fe_xO/NC before and after 5500 cycles.

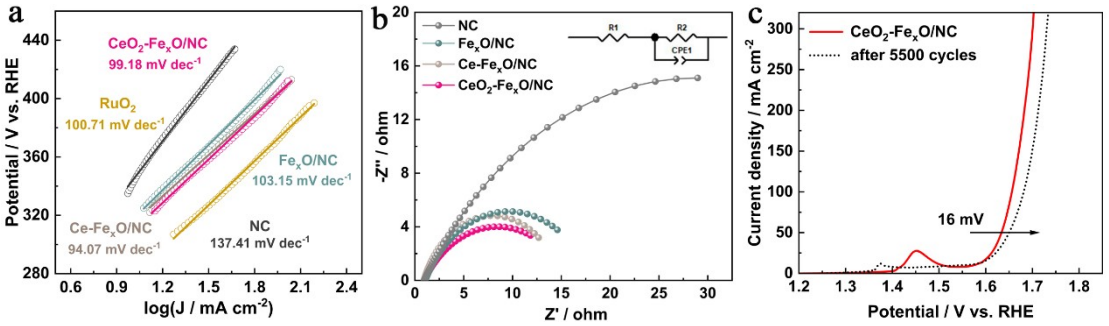

Fig. S8. OER performance: (a) Tafel fitting plot, (b) Impedance spectrum, and (c) Polarization curves of CeO_2-Fe_xO/NC before and after 5500 cycles.

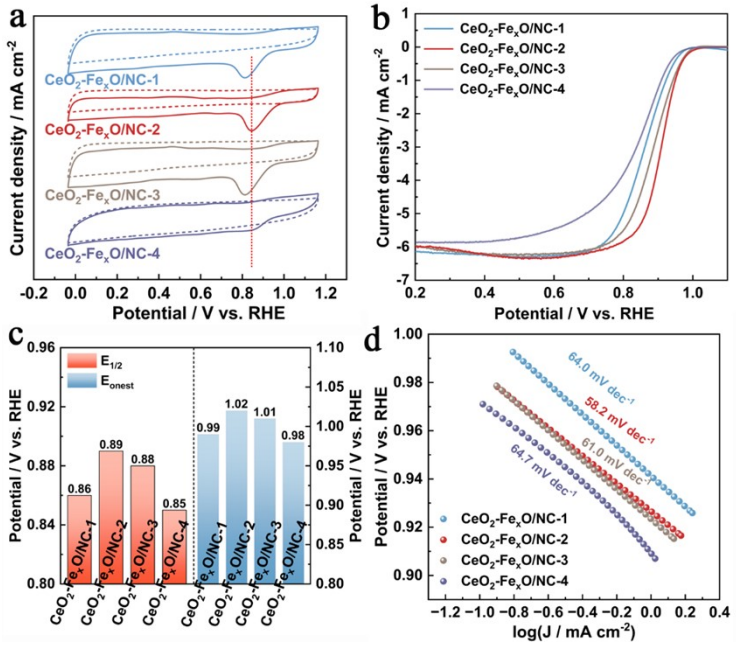

Fig. S9. CeO_2-Fe_xO/NC-1, CeO_2-Fe_xO/NC-2, CeO_2-Fe_xO/NC-3, and CeO_2-Fe_xO/NC-4 samples in 0.1 M KOH: (a) CV curves, (b) LSV curves, (c) E_{onest} and $E_{1/2}$, and (d) Tafel slope fitting plot.

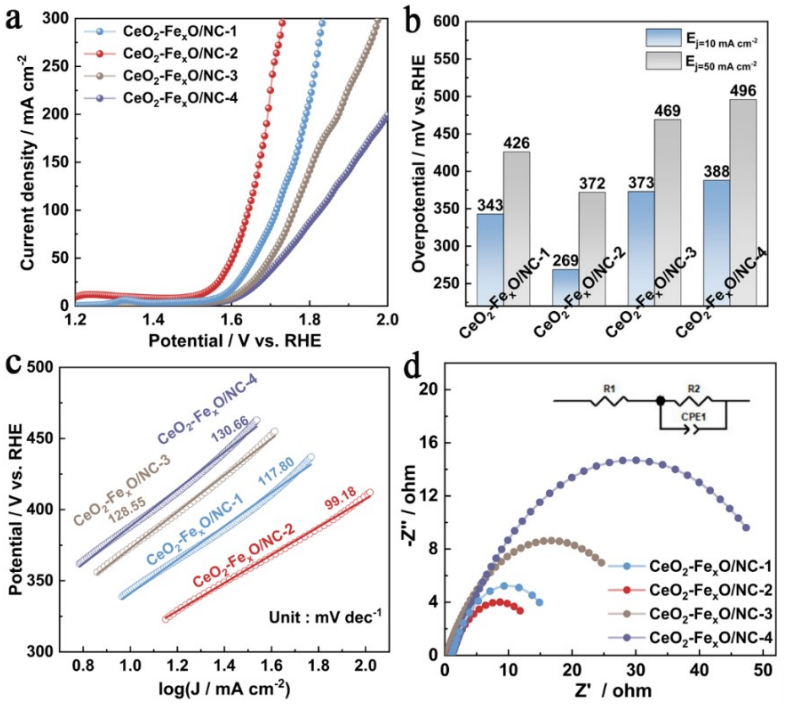

Fig. S10. CeO_2-Fe_xO/NC-1, CeO_2-Fe_xO/NC-2, CeO_2-Fe_xO/NC-3, and CeO_2-Fe_xO/NC-4 samples in 1.0 M KOH: (a) LSV curves, (b) Overpotential, (c) Tafel fitting plot, and (d) Impedance spectra at 1.57 V vs. RHE.

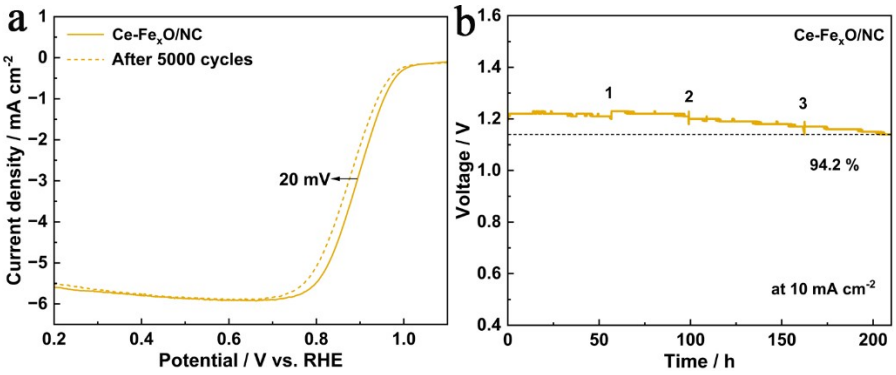

Fig. S11. Ce-Fe_xO/NC sample: (a) Polarization curves before and after 5500 CV cycles, (b) ZAB discharge curve.

Table S2. Fitting results of diffraction angle and graphene spacing for XRD

Samples	CeO_2-Fe_xO/NC	Ce-Fe_xO/NC	Fe_xO/NC	NC
Diffraction angle (°)	25.09	25.05	24.86	24.59
Graphene spacing (Å)	3.54	3.55	3.58	3.62

Table S3. Nitrogen content of different samples in XPS analysis

Samples	CeO_2-Fe_xO/NC	Ce-Fe_xO/NC	Fe_xO/NC
Content (%)	5.45	4.62	4.34

Table S4. The comparison of the ORR and OER performance of CeO_2-Fe_xO/NC catalyst sample with the results reported in recent literature.

Catalysts	**$E_{j=10}$ mA cm^{-2} (V vs. RHE)**	**$E_{1/2}$ (V vs. RHE)**	**ΔE (V vs. RHE)**	**Reference**
CeO_2-Fe_xO/NC	1.51	0.89	0.62	This work
Co_4N@d-NCNWs/D	1.57	0.83	0.74	[1]
Co-CeO_2/C	1.61	0.86	0.75	[2]
FeNi/TNCF-2	1.53	0.88	0.65	[3]
FeCo/N-CF	1.67	0.89	0.78	[4]
CuNCs/Fe_3N-NPCF	1.51	0.85	0.66	[5]
CoCu/N-CNS-2	1.47	0.84	0.63	[6]
SD-Fe-N/C	1.57	0.85	0.72	[7]
CeO_2@$CoSe_2$-NCs	1.55	0.76	0.79	[8]
CeO_2-FeNC-5	1.55	0.90	0.65	[9]
FeCo–NCps	1.61	0.85	0.76	[10]
Cu NDs/Fe_2O_3-NPCs	1.55	0.85	0.7	[11]
FeCo/Se-CNT	1.57	0.90	0.67	[12]

Table S5. The comparison of the ZAB performance of CeO_2-Fe_xO/NC catalyst with other catalysts reported in recent literature.

Catalysts	Specific capacity (mAh g^{-1})	Power density (mW cm^{-2})	Current density (mA cm^{-2})	Reference
CeO_2-Fe_xO/NC	743.0	108	10	This work
Co-FeCo/N-G	609	82	10	[13]
SnCe-ZSM	-	98	-	[14]
NiFe@N-CFs	719	102	5	[15]
FePc@CeO_2/N SCNF	827.8	83.1	20	[16]
Co-Fe-P-Se/NC	708	104	5	[17]
FePc@N,P-DC	585	120	10	[18]
(Fe,Co)-SA/CS	819.6	85	5	[19]
P-FeCo/NC	760.39	115	10	[20]
Fe@C-NG/CNTs	682	101.2	10	[21]

References:

1. F. Zhang, X. Liu, Y. Chen, M. Tian, T. Yang, J. Zhang, S. Gao, Chin. Chem. Lett. 2023, **34,** 108142.

2.Z. Liu, J. Wan, M. Li, Z. Shi, J. Liu, Y. Tang, Nanoscale 2022, **14,** 1997-2003.

3.M. Wang, S. Ji, H. Wang, X. Wang, V. Linkov, R. Wang, Small 2022, **18,** 2204474.

4.Y. Deng, J. Zheng, B. Liu, H. Li, M. Yang, Z. Wang, J. Energy Chem 2023, **76,** 470-478.

5.Q. Dong, G. Li, F. Liu, J. Ren, H. Wang, R. Wang, Appl. Catal., B 2023, **326,** 122415.

6.J. Kuang, Y. Shen, Y. Zhang, J. Yao, J. Du, S. Yang, S. Zhang, Y. Fang, X. Cai, Small 2023, **19,** 2207413.

7.J.-C. Li, Y. Meng, H. Zhong, L. Zhang, S. Ding, Z. Lyu, S. P. Beckman, P.-X. Hou, Y. Mei, H.-M. Cheng, C. Liu, Carbon 2023, **205,** 302-309.

8.Q. Guo, Y. Li, Z. Xu, R. Liu, Adv. Energy Mater. 2024, 2403744.

9.Y. Huang, Y. Zhang, J. Hao, Y. Wang, J. Yu, Y. Liu, Z. Tian, T.-S. Chan, M. Liu, W. Li, J. Li, J. Colloid Interface Sci. 2022, **628,** 1067-1076.

10.J. Liu, T. He, Q. Wang, Z. Zhou, Y. Zhang, H. Wu, Q. Li, J. Zheng, Z. Sun, Y. Lei, J. Ma, Y. Zhang, J. Mater. Chem. A. 2019, **7,** 12451-12456.

11.Q. Dong, S. Ji, H. Wang, V. Linkov, R. Wang, ACS Appl. Mater. Interfaces 2022, **14,** 51222-51233.

12.H. Zhang, M. Zhao, H. Liu, S. Shi, Z. Wang, B. Zhang, L. Song, J. Shang, Y. Yang, C. Ma, L. Zheng, Y. Han, W. Huang, Nano Lett. 2021, **21,** 2255-2264.

13.Q. Jin, B. Ren, J. Chen, H. Cui, C. Wang, Appl. Catal., B 2019, **256,** 117887.

14.G. Meng, Z. Chang, X. Cui, H. Tian, Z. Ma, L. Peng, Y. Chen, C. Chen, J. Shi, Chem. Eng. J. 2021, **417,** 127913.

15.Y. Niu, X. Teng, S. Gong, Z. Chen, J. Mater. Chem. A. 2020, **8,** 13725-13734.

16.S. Tao, S. Xiang, Y. Yu, H. Lan, C. Liu, J. Zhang, Carbon 2024, **220,** 118893.

17.H. Wu, J. Wang, J. Yan, Z. Wu, W. Jin, Nanoscale **2019, 11,** 20144-20150.

18.W. Cheng, P. Yuan, Z. Lv, Y. Guo, Y. Qiao, X. Xue, X. Liu, W. Bai, K. Wang, Q. Xu, J. Zhang, Appl. Catal., B 2020, **260,** 118198.

19.V. Jose, H. Hu, E. Edison, W. Manalastas Jr., H. Ren, P. Kidkhunthod, S. Sreejith, A. Jayakumar, J. M. V. Nsanzimana, M. Srinivasan, J. Choi, J.-M. Lee, Small Methods 2021, **5,** 2000751.

20.N. Wang, R. Mei, L. Chen, T. Yang, Z. Chen, X. Lin, Q. Liu, Small 2024, **20,** 2400327.

21.Q. Wang, Y. Lei, Z. Chen, N. Wu, Y. Wang, B. Wang, Y. Wang, J. Mater. Chem. A. 2018, **6,** 516-526.